JOURNAL OF CATALYSIS **172,** 322–335 (1997)
ARTICLE NO. CA971881

Palladium–Silver Sol-Gel Catalysts for Selective Hydrodechlorination of 1,2-Dichloroethane into Ethylene

I. Synthesis and Characterization

Benoît Heinrichs,*[,1] Patrice Delhez,* Jean-Paul Schoebrechts,† and Jean-Paul Pirard*

*Laboratoire de Génie Chimique, Institut de Chimie-B6a, Université de Liège, Sart-Tilman, B-4000 Liège, Belgium; and †Laboratoire Central, Solvay, S.A., Rue de Ransbeek, 310, B-1120 Brussels, Belgium

Received April 29, 1997; revised August 11, 1997; accepted August 13, 1997

Low-density xerogel Pd–Ag/SiO_2 catalysts were prepared by a cogelation of tetraethoxysilane with organically substituted alkoxides capable of forming chelates with palladium and silver ions, followed by a drying under vacuum, a calcination, and a reduction. The resulting Pd–Ag alloy particles have diameters of about 2–3 nm and are dispersed inside the silica particles which exhibit a monodisperse micropore size distribution centered at 0.8 nm. At low silver loading, the composition of the bimetallic particles is almost identical to the overall composition, but when this loading is increased, the percentage of silver in the alloy particles is appreciably lower than the overall percentage. In all bimetallic samples, a few large pure silver particles are observed. When dried under vacuum, the xerogels exhibit a texture similar to that of aerogels dried under supercritical conditions with pore volumes in the range 2–6 cm^3/g and pores ranging from micro- to macropores of several hundred nanometers. When the silver loading is increased, xerogels containing palladium show aggregates of increasingly interpenetrated silica particles. This is explained by an aggregation, during the gelation reaction, of colliding SiO_2 particles which is limited by an increasingly slow sticking reaction due to the growing basicity in the precursor solution when the concentrations of Ag and associated compounds are increased. During thermal treatments, the Pd–Ag alloy seems to form by the migration, through the porous network, of silver which finally alloys with Pd crystallites trapped inside SiO_2 particles. Whereas ethane is the main product when hydrodechlorination of 1,2-dichloroethane is performed over pure palladium, the dilution of this active metal by silver leads to a strong increase in ethylene selectivity.

INTRODUCTION

Chlorinated wastes generated by industrial processes are generally eliminated by thermal or catalytic incineration (1–3). Kalnes and James (4) have shown, however, that, for wastes such as polychlorobiphenyl compounds and halogenated petrochemical by-products such as chlorinated alkanes, hydrodechlorination and reuse provide a more economical solution than incineration. Studies of catalytic hydrodechlorination reported in the literature are concerned essentially with the hydrogenolysis of the carbon–chlorine bond: $\equiv C-Cl + H_2 \rightarrow \equiv C-H + HCl$ (5–7). Metals from Group VIII are mostly used. In the case of 1,2-dichloroethane, which is examined in this work, this reaction would then produce ethane. However, Ito *et al.* (8) recently demonstrated the ability of bimetallic catalysts, composed of metals from Groups VIII and IB, to convert chlorinated alkanes into less-chlorinated or unchlorinated alkenes. This new process is very attractive, because alkenes are raw materials for numerous industrial reactions.

The sol-gel method was used by several authors in order to obtain monometallic or bimetallic catalyst particles finely dispersed on a mineral support. For example, López, Gómez, and co-workers synthesized Ru/SiO_2 (9–12), Pd/SiO_2 (13), and Pt/SiO_2 (14) catalysts by addition of the metal of interest in the form of a salt ($RuCl_3$, $PdCl_2$, H_2PtCl_6) in the initial solution which contains tetraethoxysilane (TEOS), water, and ammonia in ethanol. A particularly interesting method to homogeneously disperse nanometer-sized metal particles in a silica matrix was studied by Schubert and co-workers (15–19). These authors used alkoxides of the type $(RO)_3Si-X-A$ in which a functional organic group A, able to form a chelate with a cation of a metal such as palladium, nickel, silver, copper, etc., is connected to the alkoxide moiety $(RO)_3Si-$ via an inert and hydrolytically stable spacer X. The cocondensation of such molecules with a network-forming reagent such as TEOS, $Si(OC_2H_5)_4$, results in materials in which the catalytic metal is anchored to the SiO_2 matrix. Schubert *et al.* applied this method to the preparation of numerous monometallic samples such as Ag/SiO_2, Co/SiO_2, Pd/SiO_2, Pt/SiO_2, etc. (15–17), and bimetallic samples such as $Cu-Ru/SiO_2$ (16, 17), $Pd-Ni/SiO_2$ (18), and $Cu-Ni/SiO_2$ (19).

In a previous study, we used this method for the preparation of Pd/SiO_2 aerogel catalysts (20). The dispersion,

[1] E-mail: b.heinrichs@ulg.ac.be.

0021-9517/97 $25.00

localization, and accessibility of palladium as well as the relation between the thermal stability and the texture of those materials were examined in detail (21). It appeared that the Pd^{2+} complex, $Pd^{2+}[NH_2–CH_2–CH_2–NH–(CH_2)_3–Si(OCH_3)_3]_2$, acts as a nucleation agent in the formation of silica particles. The resulting catalysts are composed of completely accessible palladium crystallites located inside silica particles. It was shown that these samples are sinterproof during hypercritical drying due to the fact that Pd crystallites cannot migrate because they are trapped in the pores of SiO_2 particles.

In the present study, we applied the same method to the preparation of bimetallic $Pd–Ag/SiO_2$ xerogel catalysts, examined their ability to selectively convert 1,2-dichloroethane into ethylene, and discussed the formation mechanisms of the gels and Pd–Ag alloys.

EXPERIMENTAL

(I) Sample Designation

Six samples containing various amounts of metals were prepared. The synthesis parameters of the gels are presented in Table 1. For each sample, X or A denote the way used to dry the gel, xerogel dried under vacuum or aerogel dried under supercritical conditions, respectively, followed by the overall atomic percentage of silver in the sample.

(II) Catalyst Preparation

Gel synthesis. The general synthesis procedure was as follows. For mixture A, to a suspension of insoluble palladium acetylacetonate powder $Pd(CH_3COCH{=}C(O–)CH_3)_2$ ($Pd(acac)_2$) in a quart of the total volume of ethanol, [3-(2-aminoethyl)aminopropyl]trimethoxysilane $H_2NCH_2CH_2NH(CH_2)_3Si(OCH_3)_3$ (EDAS) is added; for mixture B, to a suspension of insoluble silver acetate powder (AgOAc) in another quart of the total volume of ethanol, 3-(aminopropyl)triethoxysilane, $H_2N(CH_2)_3Si(OC_2H_5)_3$ (AS) is added. For the monometallic samples X0 and X100, only one mixture was prepared in half the total volume of ethanol. Mixtures A and B were stirred at ambient temperature in closed vessels until a clear solution was obtained after approximately 1 h (formation of palladium and silver complexes (15, 19)), after which they were mixed together. Tetraethoxysilane (TEOS) was then added. Finally, a solution containing aqueous 0.18 N NH_3 in the remaining ethanol, was slowly added under vigorous stirring. The vessel was then closed tightly and heated to 70°C for 3 days (gelation and aging (22)). In all gels, the dilution molar ratio $R = C_2H_5OH/(TEOS + EDAS + AS) = 10$, the hydrolysis molar ratio $H = H_2O/(TEOS + 3/4EDAS + 3/4AS) = 5$ (the factor 3/4 is due to the fact that EDAS and AS contain only three hydrolysable groups, while TEOS contains four hydrolysable groups), and the molar ratios EDAS/Pd and AS/Ag = 2 (value chosen by Breitscheidel *et al.* (15)). In the pure silver sample X100, the addition of EDAS was necessary to obtain gelation of the solution.

Drying. After aging, gels X0 to X100 were dried under vacuum according to the following procedure: the vessels were opened and put into a drying oven heated to 80°C, and the pressure was slowly decreased (to prevent gel bursting) to the minimum value of 1200 Pa after 20 h. The drying oven was maintained under these conditions for 24 h and was then heated at 150°C for 72 h. The resulting samples are xerogels (22). Gel A67, which is identical to gel X67, was dried in an autoclave under supercritical conditions for the interstitial liquid (21). This drying was performed as follows: the opened vessel was filled with ethanol and inserted into the autoclave which was then pressurized at 5 MPa with nitrogen. The temperature was increased to 327°C at a rate of 2°C/min, and the pressure was maintained at 13 MPa as soon as this value was reached. After 2 h at 327°C, the pressure was released, the heating was shut off, and the autoclave was flushed with nitrogen. Sample A67 is an aerogel.

Calcination. In order to choose a calcination temperature but also to examine their behavior in air at high temperature, all samples were submitted, just after drying, to thermogravimetric analysis (TGA) under air coupled with differential scanning calorimetry (DSC) on a Setaram TG-DSC 111 instrument. The conditions of calcination were as follows: the sample was heated to 400°C at a rate of 120°C/h

TABLE 1

Synthesis Parameters of the Gels

Catalyst	$Pd(acac)_2$ (mmol)	Ag(OAc) (mmol)	EDAS (mmol)	AS (mmol)	TEOS (mmol)	H_2O (mmol)	NH_3 (mmol)	C_2H_5OH (mmol)	Pd (wt%)	Ag (wt%)	Gel time (min)
X0	2.69	0	5.36	0	307	1554	4.93	3122	1.5	0	26
X33	2.70	1.35	5.41	2.77	304	1549	4.91	3100	1.5	0.75	15
X50	2.75	2.70	5.48	5.40	303	1474	4.67	3138	1.5	1.5	15
X67	2.76	5.48	5.55	11.06	296	1540	4.88	3121	1.5	3.0	13
X100	0	2.65	5.32	5.32	302	1549	4.91	3124	0	1.5	30
A67	2.77	5.47	5.55	11.06	296	1540	4.88	3121	1.5	3.0	12

under flowing air (1.8 Nl/h); this temperature in air (9 Nl/h) was maintained for 12 h.

Reduction. Before characterization, the catalyst was heated to 350°C at a rate of 350°C/h under flowing H_2 (20 Nl/h) and maintained at this temperature for 3 h (same flow).

(III) Catalyst Characterization

The composition and size of the metallic particles were examined by X-ray diffraction (XRD), transmission electron microscopy (TEM), and scanning transmission electron microscopy coupled with energy dispersive X-ray spectroscopy (STEM-EDX). The XRD patterns were obtained with hand-pressed samples mounted on a Philips PW1050 goniometer. A copper anode X-ray tube (Philips PW1729) was used as the radiation source. TEM and STEM-EDX analyses were performed on a Siemens Elmiskop 102 transmission electron microscope. Suitable transmission samples were prepared by means of impregnation of the xero- or aerogel with an epoxy resin (eurepox 710) to which an amine was added to serve as a hardener. Hardening went on for 48 h, after which a 60-nm slice was cut up with a Reichert Supernova ultramicrotome.

Texture was examined in detail by nitrogen adsorption at 77 K on a Fisons Sorptomatic 1990, mercury porosimetry on a Carlo Erba Porosimeter 2000 (which operates up to 200 MPa), and helium pycnometry on a Micromeritics AccuPyc 1330. Scanning electron microscopy (SEM) with a Jeol JSM-840 A microscope and transmission electron microscopy (see above) were also used.

(IV) Catalytic Experiments

The hydrodechlorination of 1,2-dichloroethane was conducted in a stainless steel tubular reactor (internal diameter, 8 mm) at a pressure of 0.3 MPa. The reactor was placed in a convection oven. A constant flow of each reactant was maintained by a Gilson piston pump for $CH_2Cl–CH_2Cl$ and Brooks mass flow controllers for H_2 and He. The mixed reactants were preheated at the reaction temperature before reaching the catalyst. The effluent was analyzed by gas chromatography (Carlo Erba GC6000 with FID) using a Chromosorb 102 packed column (Alltech, 5 m, 1/8″, 80/100 mesh).

Prior to each experiment, the catalyst was reduced *in situ* at atmospheric pressure in flowing H_2 (2 Nl/h) while being heated to 350°C at a rate of 350°C/h and was maintained at this temperature for 3 h. After reduction, the catalyst was cooled in H_2 to the desired initial reaction temperature of 200°C.

For each catalytic experiment, 0.11 g of catalyst pellets, sieved between 250 and 500 μm, were used. The total flow of the reactant mixture was 40 Nl/h and consisted of $CH_2Cl–CH_2Cl$ (1 Nl/h), H_2 (2 Nl/h), and He (37 Nl/h). The temperature was kept successively at 200, 250, 300, 350, and 300°C. The effluent was analyzed every hour and three analyses were made at each temperature (five for the last level).

RESULTS

(I) Composition, Size, and Localization of Metal Particles

Figure 1 shows the diffractograms obtained for the bimetallic samples. Between the (111) Bragg lines of pure

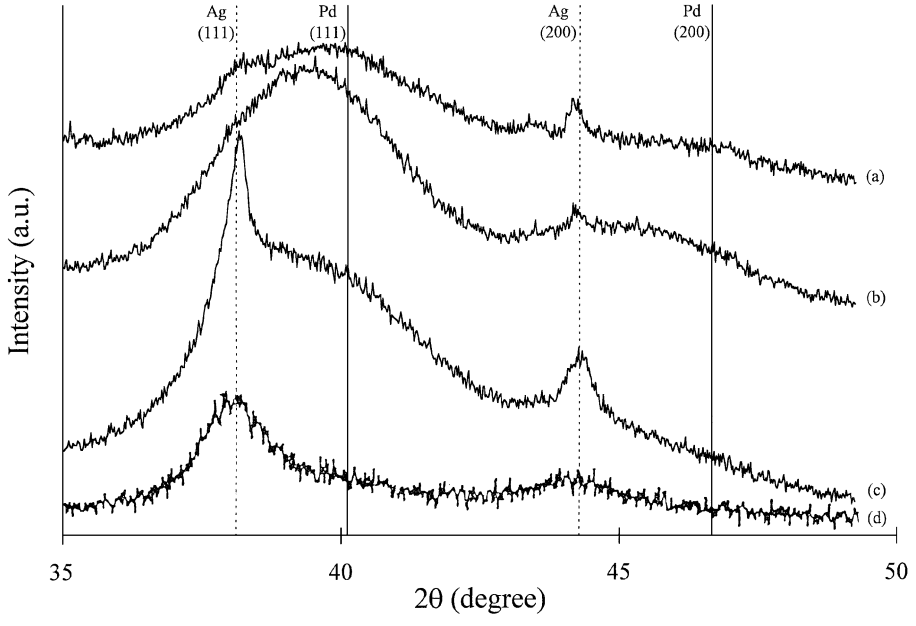

FIG. 1. X-ray diffraction patterns of Pd–Ag samples: (a) X33, (b) X50, (c) X67, (d) A67.

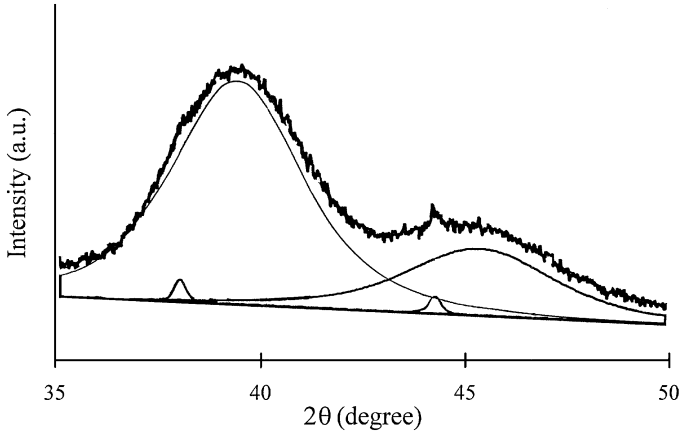

FIG. 2. Deconvolution into four peaks of the XRD pattern of sample X50 (Fig. 1b).

Pd and Ag, xerogels X33, X50, and X67 (Figs. 1a–1c) exhibit a broad peak which demonstrates the presence of a solid solution (SS). After spectra deconvolution, as shown in Fig. 2 in the case of sample X50, the (200) broad peak appears. The presence of unalloyed silver is clearly evident in sample X67, two peaks being characteristic of this metal (Fig. 1c). In xerogels X33 and X50, the presence of pure silver is also demonstrated by the shoulder at the left of the (111) SS peak and the small (200) Ag peak (Figs. 1a, 1b, and 2). The composition of the solid solution was calculated from the unit cell parameter corresponding to the SS peak (23). Results in Table 2 indicate that the composition of the bimetallic particles (phase 1) is nearly the same as the overall composition in xerogel X33, but deviates increasingly from the overall composition for increasing Ag content. The main reason for this composition gap is probably the presence of a pure silver phase but, as explained by El Hamdaoui *et al.* (24), the shift toward a lower silver percentage may also result from surface enrichment with Ag. This enrichment was indeed observed by numerous authors who examined the surface of Pd–Ag alloys using various techniques (25–27). It results from the lower surface energy of silver with respect to palladium (28). The very wide SS peaks are due to the small size of the particles and/or to a distribution of composition (24). With the assumption that all the bimetallic particles have the same Pd–Ag composition, their size can be calculated from the peak broadening (23). Bimetallic particles in xerogels X33, X50, and X67 are found to be finely dispersed, whereas pure silver particles in these samples are much larger. The XRD pattern of bimetallic aerogel A67 (Fig. 1d) seems to show only the presence of pure silver particles. Nevertheless, a nearly pure palladium phase, scarcely distinguishable in the raw spectrum, appears after deconvolution. Aerogel A67 therefore exhibits an almost total segregation of palladium and silver. As in the xerogels, the pure Ag particles are larger than the Pd-containing particles.

TEM micrographs show that all xero- and aerogels containing palladium exhibit metal particles distributed in two families of different size (see Table 2 and examples in Figs. 3–5 with samples X0, X67, and A67). Bimetallic xerogels X33, X50, X67, and aerogel A67 exhibit small and large particles with diameters of 2 to 3 nm and 7 to 10 nm, respectively. It appears that there are more large particles in A67 than in X67 and in X67 than in X33 and X50. In the pure Pd sample X0 (Fig. 3), small particles are about the same size (2.3 nm) but large particles are much larger, with a mean diameter of 28 nm. The pure silver catalyst X100 exhibits a broad distribution of metal particle sizes from 1 to 20 nm (Fig. 6). Except in X100, it appears that the catalysts are composed of silica particles arranged in strings or aggregates, and although TEM gives only a 2D view, it seems that small metal particles are located inside silica particles, whereas large metal particles are located at their surface.

(II) Catalyst Texture

The texture examination by nitrogen adsorption (quantitatively applicable for pores smaller than 30 nm) as well as mercury porosimetry (applicable for pores larger than 7.5 nm) shows that the catalysts prepared in this work exhibit a very broad range of pore sizes. Results are presented

TABLE 2

Characterization of Metallic Phases

	Ag/(Pd + Ag) (at.%)			Particle size (nm)				
		XRD		XRD		TEM		$T_{combustion}$ (°C)
Catalyst	Overall	Phase 1	Phase 2	Phase 1	Phase 2	Small	Large	TG-DSC
X0	0	0	—	7.7	—	2.3	28	256
X33	33	31	100	1.9	>30	2.4	9	272
X50	50	43	100	2.1	>30	3.0	7	289
X67	67	46	100	2.0	18	3.0	10	294
X100	100	100	—	10.3	—	from 1 to 20		359
A67	67	8	100	2.7	6	2.4	10	x

Note. —, nonexistent. x, not measured.

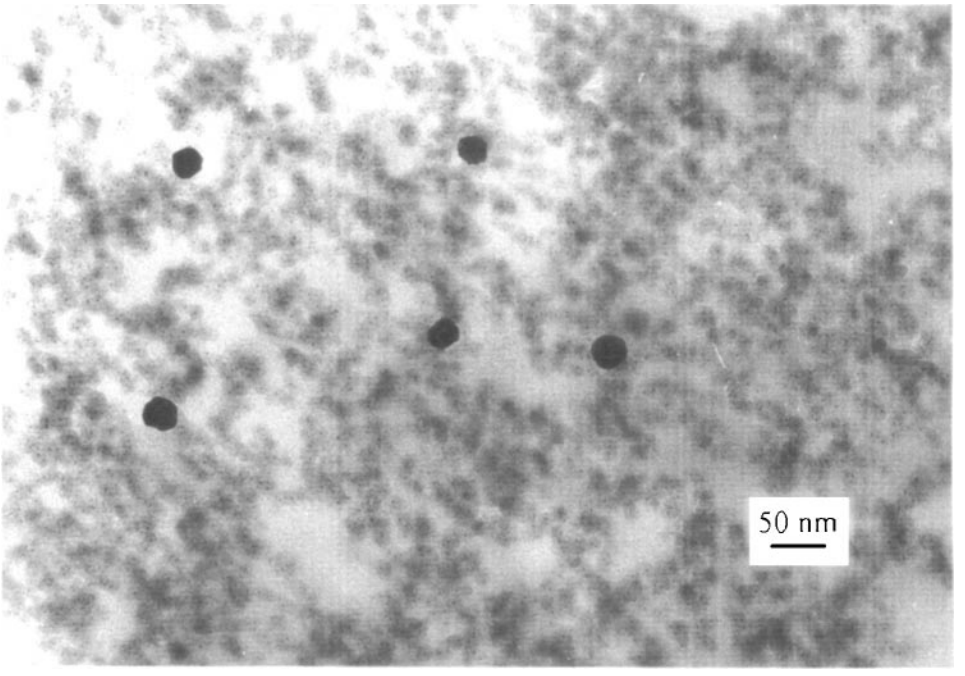

FIG. 3. TEM micrograph of sample X0 (original magnification, 200000).

in Table 3 and Figs. 8–10. The nitrogen adsorption isotherms of all xerogels, an example of which is given in Fig. 8 with sample X67, are similar but do not clearly belong to one of the five theoretical types defined in the classification established by Brunauer *et al.* (29, 30). At low relative pressure, a sharp increase of the adsorbed volume is followed by a plateau which corresponds to type I isotherm which is characteristic of microporous adsorbents. At high pressure, the adsorbed volume increases quickly like in type II or III isotherms which are characteristic of macroporous adsorbents. Moreover, all catalysts exhibit an adsorption–desorption hysteresis loop which is

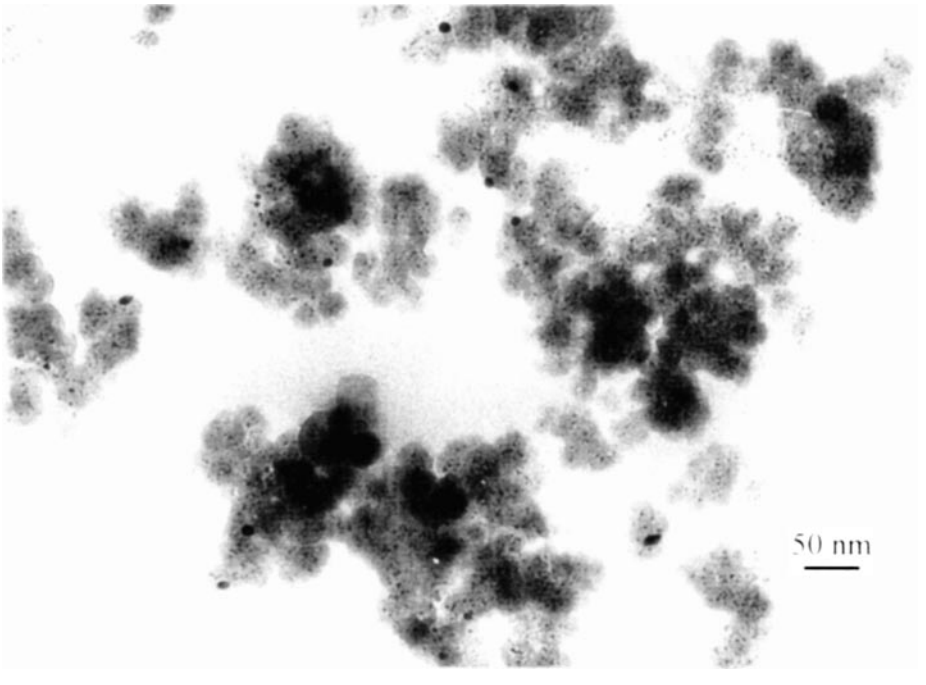

FIG. 4. TEM micrograph of sample X67 (original magnification, 200000).

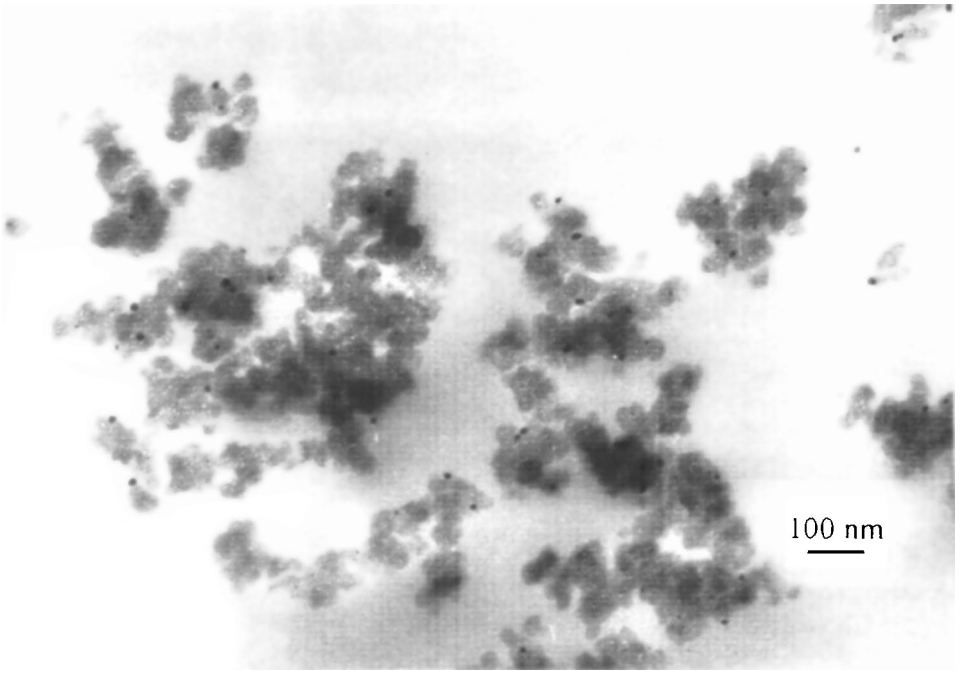

FIG. 5. TEM micrograph of sample A67 (original magnification, 100000).

characteristic of capillary condensation in mesopores. In the case of aerogel A67, the low-pressure part of the isotherm does not exhibit the steep increase of the adsorbed volume characteristic of micropores (Fig. 8). The xerogel samples (Figs. 9a–9e) then contain micropores (size < 2 nm), mesopores (2 nm < size < 50 nm), and macropores (size > 50 nm) (31) all at the same time whereas aerogel A67 (Fig. 9f) contains only mesopores and macropores. The cumulated distributions over the complete pore size range shown in Fig. 9 were obtained by applying a combination of various

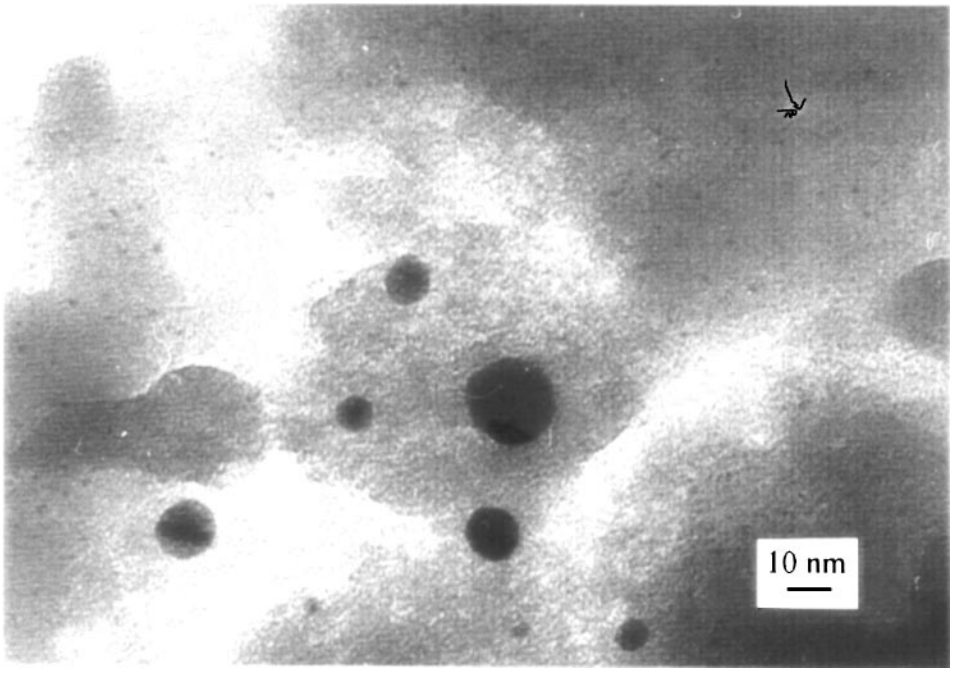

FIG. 6. TEM micrograph of sample X100 (original magnification, 800000).

TABLE 3

Texture of Catalysts

Catalyst	S_{BET} (m^2/g)	S_t (m^2/g)	S_w (m^2/g)	V_p (cm^3/g)	V_{Hg} (cm^3/g)	ρ_{app} (g/cm^3)
X0	485	488	240	1.1	2.5	2.14
X33	379	381	176	0.8	4.3	2.14
X50	290	292	138	0.6	4.7	2.19
X67	321	322	98	0.5	6.1	2.22
X100	193	194	—	0.2	4.9	2.14
A67	60	61	61	0.6	9.2	2.20

Note. S_{BET}, specific surface area obtained by the BET method; S_t, specific surface area obtained from the slope before the downward deviation in the *t*-plot; S_w, specific surface area obtained from the slop after the downward deviation in the *t*-plot; V_p, specific liquid volume adsorbed at saturation pressure of N_2; V_{Hg}, specific volume measured by mercury porosimetry; ρ_{app}, apparent density measured by helium pycnometry. —, not measurable.

methods to their respective validity domains and by additioning the porous volumes corresponding to those domains. The distributions of micropores were calculated by Brunauer's method applied to the *t*-plots derived from nitrogen adsorption isotherms (32, 33). The *t*-plots of xerogels X0, X33, X50, and X67 are similar (Fig. 10): they always show a sharp downward deviation around $t = 0.4$ nm, which indicates filling of nearly monodisperse micropores followed by an upward deviation because of capillary condensation in mesopores. Such behavior was already observed for Pd/SiO_2 cogelled aerogel catalysts dried under supercritical conditions in a previous study (21). It is particularly interesting to observe this behavior in xerogels dried under vacuum, too. As for Pd/SiO_2 aerogel catalysts, Brunauer's method applied to the downward deviation leads to a very narrow micropore size distribution (expressed as percentage of micropore surface per nanometer) centered on half a pore width $w/2 = t$ of about 0.4 nm (Fig. 10). The slopes on both sides of the downward deviation, but before the upward deviation, in the *t*-plots allow us to calculate the surfaces S_t, quasi-equal to the specific surface area S_{BET}, and S_w (30), the meaning of which will be discussed in the next section (Table 3). Contrary to Pd-containing xerogels, the pure silver sample X100 (Fig. 9e) exhibits a broad micropore size distribution from 0.7 to 2 nm, and aerogel A67 (Fig. 9f) does not contain any micropores (no downward deviation in the *t*-plot). These differences appear clearly in the micropore domain of Fig. 9: samples X0, X33, X50, and X67 are characterized by a steep volume increase around 0.8 nm followed by a plateau; sample X100 shows a continuous increase from 0.7 to 2 nm; and the distribution of sample A67 begins after 2 nm.

The distributions of mesopores smaller than 7.5 nm were calculated by the Broekhoff–de Boer method based on nitrogen capillary condensation (34–36). Mesopores larger than 7.5 nm and macropores were examined by mercury porosimetry. The application of this technique to aerogels and low-density xerogels was studied in detail by Pirard *et al.* (37–39). The pore volumes V_{Hg} of xerogels X0 to X100 are in the same order of magnitude as the pore volume of aerogel A67 (Table 3) or other aerogels described in the

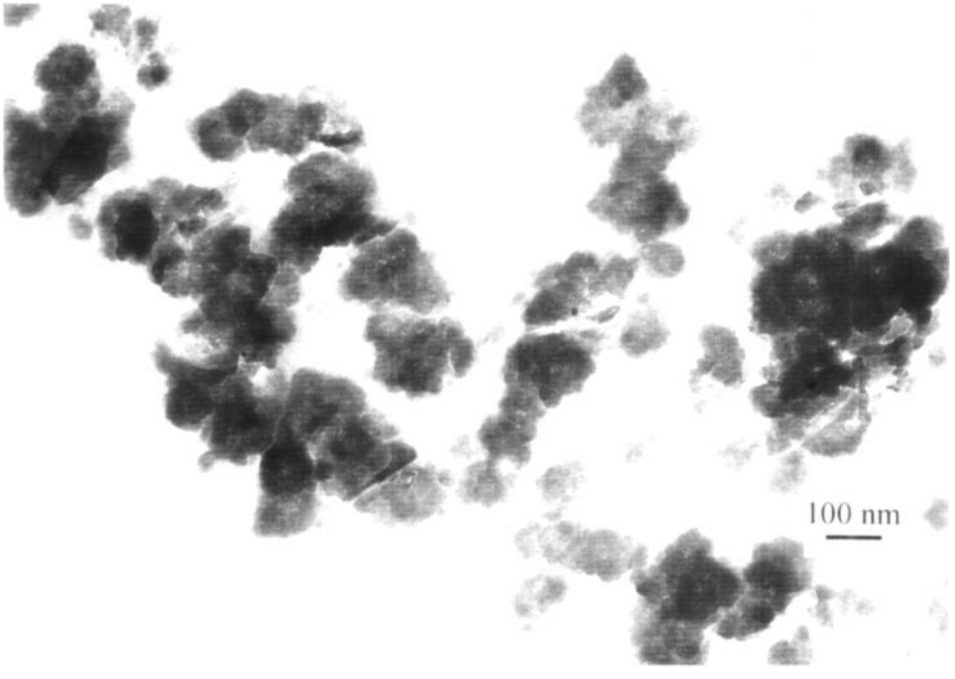

FIG. 7. TEM micrograph of sample X100 (original magnification, 100000).

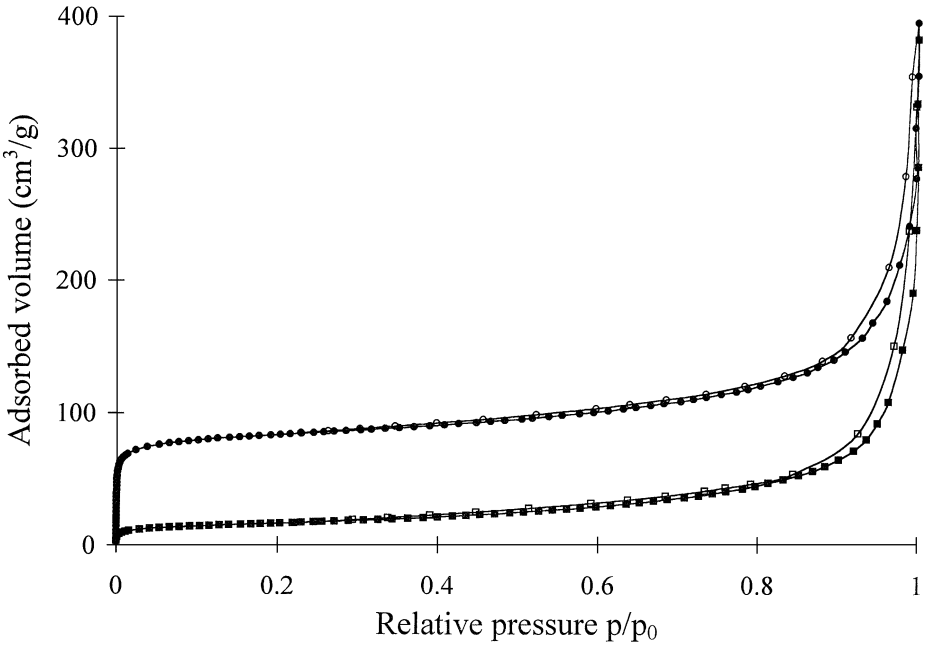

FIG. 8. N_2 adsorption–desorption isotherms: (●) X67 adsorption, (○) X67 desorption, (■) A67 adsorption, (□) A67 desorption.

literature (40). For this reason, those xerogels are called "low-density xerogels." Submitted to an increasing mercury pressure, those materials exhibit two successive behaviors: at low pressure, they behave as an aerogel and collapse under the isostatic pressure, and above a critical pressure, which is characteristic of the material composition and microstructure, mercury can enter into the network of small pores not destroyed during the compression at low pressure. Two models must then be used in order to calculate the pore size distribution from mercury porosimetry: Washburn's model describing the mercury intrusion in small pores (30) and Pirard's model describing the collapse of larger pores (37, 38). The results of this calculation are shown in the part of Fig. 9 relative to big mesopores and macropores. One has to remark that N_2 adsorption and Hg porosimetry have an overlapping region between 7.5 (with a porosimeter operating up to 200 MPa) and 30 nm. In this study, the value of 7.5 nm was chosen for the connection

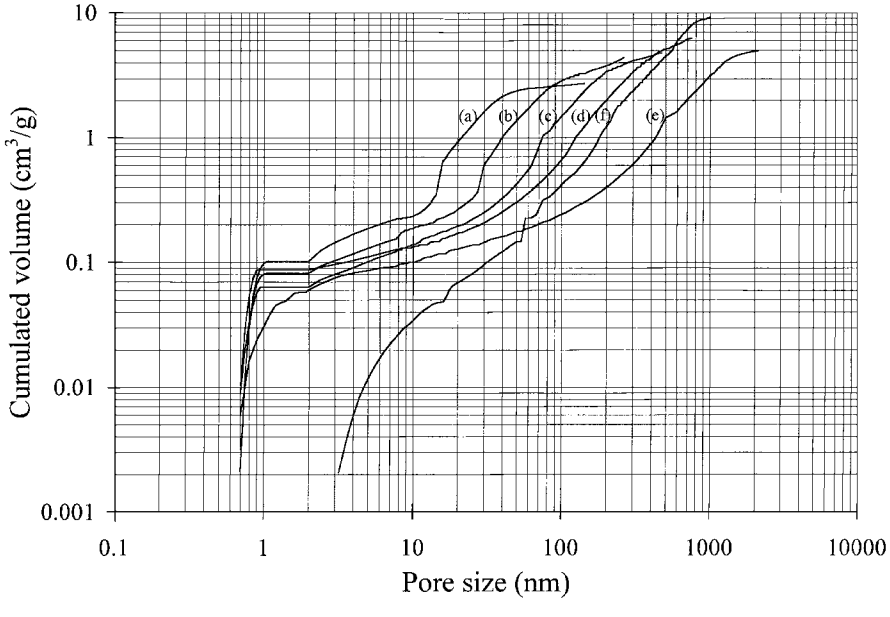

FIG. 9. Pore size distributions: (a) X0, (b) X33, (c) X50, (d) X67, (e) X100, (f) A67.

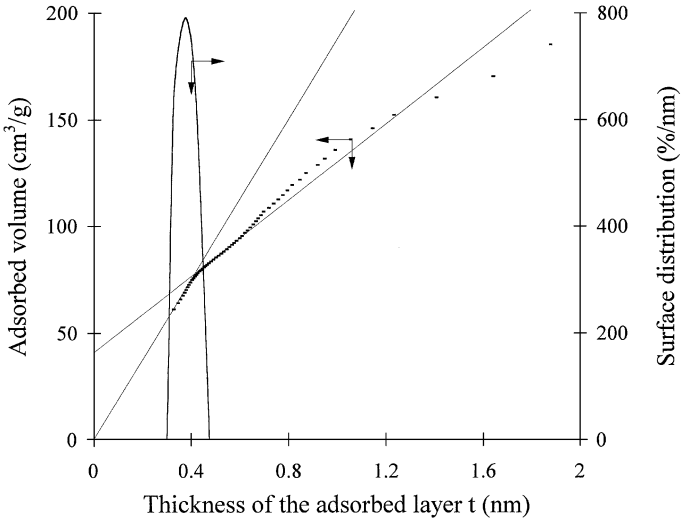

FIG. 10. *t*-Plot and micropore size distribution of sample X50.

between the two methods but other connecting values were tried. No important differences were observed but, in the overlapping region, cumulated volumes calculated by N_2 adsorption were always slightly lower than those calculated by Hg porosimetry.

In summary, in the range of meso- and macropores, one observes that all samples exhibit a broad distribution and that for xerogels (Figs. 9a–9e) this distribution shifts toward the large pores from X0 to X100. This result is reinforced by the examination of samples by SEM. In each xerogel, this technique allows one to see the largest pores, the size of which is found to increase from X0 to X100.

The catalyst apparent density (ρ_{app}) was measured by helium pycnometry. Values given in Table 3 are in good agreement with the true density of dried alkoxy-derived silica gels (41) (slightly higher because of the presence of Pd and/or Ag); this means that there are no closed pores inside the catalyst structure.

The texture was also examined by TEM. Micrographs of samples X0, X33, X50, and X67 show that when Ag loading is increased, the xerogel structure evolves from an arrangement of silica particles in strings to an arrangement in aggregates which become more compact (examples in Figs. 3 and 4 with samples X0 and X67). Aerogel A67 (Fig. 5) exhibits dense aggregates comparable in size to X67, and xerogel X100 contains much larger aggregates where silica particles do not appear clearly as is the case in Pd-containing samples (Figs. 6 and 7). The influence of synthesis parameters on xero- and aerogel structure will be discussed below.

(III) Catalytic Experiments

Pure silver xerogel X100 and aerogel A67 were completely inactive for the hydrodechlorination of 1,2-dichloroethane. On the contrary, xerogels X0, X33, X50, and X67 convert $CH_2Cl–CH_2Cl$ with an increasing selectivity in ethylene as shown in Fig. 11. The pure palladium sample X0

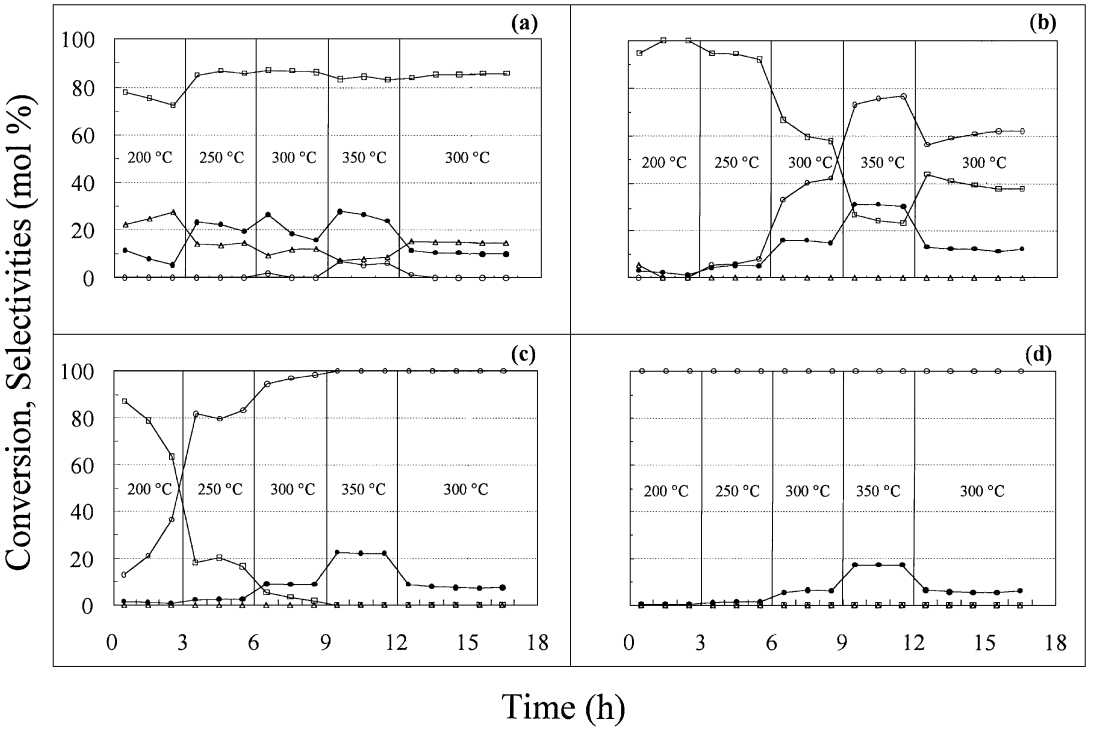

FIG. 11. Hydrodechlorination of 1,2-dichloroethane: (a) X0, (b) X33, (c) X50, (d) X67. (●) $CH_2Cl–CH_2Cl$ conversion, (○) C_2H_4 selectivity, (□) C_2H_6 selectivity, (△) $CH_3–CH_2Cl$ selectivity.

(Fig. 11a) mainly produces ethane with a selectivity of about 85%. Ethyl chloride CH_3–CH_2Cl, which is not observed with the other catalyst (except for a very small amount with X33 for the first point at 200°C), is the secondary product. Only at 350°C is C_2H_4 produced with a selectivity of about 6%. A strong deactivation is observed at all temperatures. After about 15 h, the catalyst seems to stabilize. The introduction of silver into the catalyst leads to a drastic change in selectivity toward C_2H_4, and when the Ag loading is high enough, this selectivity reaches 100%. With catalyst X67 (Fig. 11d), C_2H_4 is the only product for the conversions reached in this test at all temperatures. Samples X33 and X50 (Figs. 11b and 11c) clearly show that ethylene selectivity increases not only with temperature, but also with time. The conversion in CH_2Cl–CH_2Cl is lowered when the silver loading is increased, which seems, however, to stabilize catalysts toward deactivation.

DISCUSSION

(I) Formation of the Gels and Structure of the Resulting Xerogels

As mentioned above, the examination of palladium-containing xerogels shows a structure with increasingly compact aggregates of silica clusters or particles as the silver loading is increased (Figs. 3 and 4 show the two extreme samples). The influence of aggregation type on the gel structure was examined by computer simulations (22). Two types were examined: monomer–cluster aggregation, in which monomers (that is, TEOS molecules) are added to clusters, and cluster–cluster aggregation, in which whole clusters diffuse and collide. In agreement with the work of Brinker and Scherer (22), who consider that the latter process is generally much more realistic, we assume that gel formation proceeds in two successive steps: (i) formation of silica particles by hydrolysis and condensation of TEOS and (ii) gelation by aggregation of those clusters. Let us consider the second step first. As explained by Brinker and Scherer (22), if the colliding clusters always stick together (sticking probability = 1), the rate of aggregation is determined by transport kinetics, and the process is known as diffusion-limited cluster–cluster aggregation (DLCCA). In this case, attachment tends to occur at the cluster periphery which leads to an open structure. In many cases, the sticking probability is much lower than unity; thus many collisions will occur before two clusters link together. This process, called reaction-limited cluster–cluster aggregation (RLCCA), allows more opportunity for the clusters to interpenetrate and leads to more compact aggregates. The RLCCA mechanism is expected to dominate when a repulsive electrostatic barrier, which decreases the sticking probability, is present between the colliding particles. In his study of the stability of aqueous silica sols, Iler indicates that pH 2 is approximately the point of zero charge (42). Above this value, the surface of the silica particles becomes negatively charged by deprotonation, and their mutual repulsion increases with pH. This repulsion effect is also observed for silica gel synthesized from TEOS in mixed alcohol–water systems: although bases as well as acids catalyze hydrolysis and condensation of TEOS, the average condensation rate (= 1/gel time) is observed to decrease at high pH because of particle stabilization toward gelation due to repulsion (22, 43). In precursor solutions of Pd-containing gels, the AgOAc and AS concentrations (the AS concentration is directly linked to that of AgOAc by the fixed molar ratio AS/AgOAc = 2) and, therefore, the basicity are increased form X0 to X67 (Table 1). Silica particles in those solutions are then characterized by a growing repulsive negative electrostatic barrier, and their aggregation is limited by an increasingly slow reaction. As explained above, this progressively slower RLCCA mechanism would have to lead to more compact aggregates. This is observed in Figs. 3 and 4 in the case of samples X0 and X67. SiO_2 particles in xerogel X0 are, indeed, interpenetrated to a limited extent and are arranged in strings, whereas in xerogel X67, they are strongly interpenetrated and arranged in dense aggregates. Xerogels X33 and X50 represent intermediate situations.

If we consider the aggregation step only, gel time is supposed to increase with the concentrations of AgOAc and AS. On the contrary, gel times reported in Table 1 indicate that gel formation is faster with increasing Ag content. This initially paradoxical result can be explained by considering the first step of gel formation, that is, the formation of silica particles by hydrolysis and condensation of TEOS. These two reactions are accelerated by an increasing basicity (22), and the gel time decrease leads to the conclusion that the formation of silica particles is probably the rate determining step in the overall process of gel formation.

The size of SiO_2 particles was measured by TEM. The values obtained for X0, X33, X50, and X67 are 13, 15, 18, and 18 nm, respectively. Due to the difficult measurements particularly when the particles are strongly interpenetrated and scarcely distinguishable, the dispersion of the values around the mean is important and those sizes cannot be considered to be significantly different. Silica particles are much larger than the monodisperse micropores of 0.8 nm detected in Pd-containing xerogels (Figs. 9a–9d), and it can be reasonably assumed, as is the case for the Pd/SiO_2 cogelled aerogels (21), that those micropores are located inside the particles. The slope of the linear part of the *t*-plot, just after the downward deviation (Fig. 10), is therefore proportional to the external surface of the SiO_2 particles, which is denoted by S_w in Table 3 (30). This external surface is observed to decrease with increasing Ag content, which is in agreement with a growing interpenetration of silica particles.

(II) Formation of Pd–Ag Alloys

It was shown previously that the complex $Pd^{2+}[H_2NCH_2CH_2NH(CH_2)_3Si(OCH_3)_3]_2$ ($Pd^{2+}(EDAS)_2$) seems to act as a nucleation agent in the formation of silica particles in an ethanolic solution containing TEOS and aqueous ammonia (21). Aerogels obtained in that study were composed of Pd crystallites with a diameter of about 2.3 nm trapped inside SiO_2 particles which exhibited a monodisperse micropore size distribution centered at 0.8 nm. This nucleation effect was observed again in the pure Pd sample X0 (Fig. 3): crystallites with the same diameter seem to be located inside SiO_2 particles exhibiting the same pore size distribution. Nevertheless, in this xerogel, large Pd crystallites with a mean diameter of 28 nm are also observed. As explained before, this might result from migration and coalescence during thermal treatments of smaller Pd particles which are not trapped inside silica particles (21, 44).

On the contrary, in the pure Ag sample, a nucleation effect by silver is not observed (Figs. 6 and 7). Whereas Pd-containing samples exhibit strings or aggregates of SiO_2 particles enclosing metal crystallites, this structure does not appear in sample X100. Silver crystallites are distributed over a broad range of sizes (Fig. 6). This distribution might result from a mechanism in which the particle size is governed by the migration and coalescence phenomenon which is notably inhibited when the size of a crystallite is matched to the diameter of the pore (21, 45, 46). Small Ag particles in X100 seem to be located inside a porous silica matrix but not inside individual silica particles having a monodisperse micropore size distribution (Figs. 6 and 9e). Unlike the palladium complex, the silver complex is, therefore, supposed not to act as a nucleation agent. In the wet gel, this molecule would be spread rather randomly through the silica network.

As shown in Figs. 3, 4, and 9a–9d, the bimetallic xerogels X33, X50, and X67 exhibit a structure similar to the pure Pd xerogel X0. TEM shows small metal crystallites which seem to be located inside silica particles with a monodisperse micropore size distribution. Several larger metal particles are also observed at the surface of the SiO_2 particles. The formation of an alloy is demonstrated by XRD, but this method also demonstrates the presence of larger pure silver particles. The alloy composition deviates appreciably from the overall composition for high contents of silver. It is interesting to compare the crystallite size determined by TEM and XRD in Table 2. For the monometallic samples X0 and X100, XRD gives an intermediate value consistent with the limits given by TEM. In the bimetallic xerogels as well as in aerogel A67, the size given by XRD for the solid solution (Phase 1 in Table 2) is always close to the size of the small particles detected by TEM. Both methods detect a second family of larger particles, and the large particles detected by XRD correspond to pure silver. These results lead to the conclusion that the small metal crystallites located inside the silica particles would be Pd–Ag alloy crystallites, whereas the large crystallites located outside the silica would consist of pure Ag. Although the sizes of small crystallites in the bimetallic xerogels X33, X50, and X67 determined by XRD and TEM are not significantly different, the sizes obtained by diffraction are systematically lower than those obtained by microscopy. This might indicate that broadening of XRD peaks corresponding to a solid solution results not only from the small size of the particles, but also from a distribution of composition (24).

The conclusion arising from the comparison of the XRD and TEM results was confirmed by an additional STEM-EDX analysis of xerogel X67 and aerogel A67. Due to their sufficient size, the focusing of the electron beam on individual large particles was possible and showed that they are composed of pure silver in both samples. On the contrary, it was not possible to focus the beam on individual small particles. Only results of groups of small particles could be obtained. Despite the very weak intensity of the signal compared to the background noise, X rays emitted by such groups were characteristic of Pd and Ag in sample X67, but in the case of sample A67, only X rays corresponding to Pd were observed.

A further examination of aerogel A67 is helpful in order to understand the mechanism of Pd–Ag alloy formation. It has been shown that this sample contains small, nearly pure Pd crystallites (8 at.% of Ag), which seem to be located inside SiO_2 particles, as well as numerous large pure Ag crystallites (Figs. 1d and 5 and Table 2). Its texture is very different from that of xerogel samples, since no micropores are present (Fig. 9f). Finally, A67 does not exhibit any activity for the hydrodechlorination of $CH_2Cl–CH_2Cl$. Since Pd has been shown to be active for hydrodechlorination (Fig. 11a), it appears that this metal in aerogel A67 is not accessible for the gas phase. On the contrary, Ag is obviously accessible (Fig. 5) but does not transform $CH_2Cl–CH_2Cl$ as shown with X100. Aerogel A67 is then probably composed of small, nearly pure palladium crystallites confined inside nonporous silica particles and large pure silver crystallites spread over their surface.

All these results are in favor of the following mechanism for the Pd–Ag alloy formation in bimetallic xerogels: in wet gels, Pd complex groups would be located inside porous SiO_2 particles because of the nucleation effect, while the Ag complex would be spread randomly through the silica network. During subsequent thermal treatments, silver would migrate through micropores inside SiO_2 particles and combine with palladium to form small alloy particles. In the course of their migration, silver atoms and/or particles could meet and form larger particles. Some of them, observed experimentally, would become too large to diffuse through the micropores and to combine with palladium. In aerogel A67, the same mechanism would probably occur,

but micropores inside SiO_2 particles would close before the majority of silver reaches palladium. This leads to the observed nearly complete segregation of the two metals. The micropore closing might be due to the condensation of Si–OH groups from the opposite walls of a micropore into Si–O–Si (22) during supercritical drying. However, this phenomenon was not observed in Pd/SiO_2 aerogels (21), and the presence of silver and associated compounds probably plays a role which is not clearly understood.

The close interaction of palladium and silver in bimetallic xerogels appeared also during the analysis of noncalcined samples by TG-DSC under air. The DSC curve of all xerogels shows a first sharp exothermic peak attributed to partial combustion of organic residues. The temperature corresponding to this peak is reported in Table 2. For Pd-containing xerogels, a growing Ag loading corresponds to a shift toward higher temperatures from 256 to 294°C. The combustion power of palladium was clearly observed during calcination of Pd/SiO_2 aerogels (21). The introduction of Ag leads to an appreciable decrease in Pd oxidation activity. This is additional indication that palladium is closely linked to silver in bimetallic xerogels. The comparison with calcination temperature, observed for the pure Ag xerogel X100 (359°C), indicates that, even in sample X67 where silver loading is the highest, the combustion catalytic activity of Pd remains important.

(III) Hydrodechlorination of 1,2-Dichloroethane

In their study of the hydrodechlorination of 1,2-dichloroethane over Rh/SiO_2 catalysts at 92–280°C, Bozzelli *et al.* (5) found that C_2H_6 and HCl are the major products of the reaction. Ethyl chloride CH_3–CH_2Cl is a minor product. These authors proposed a reaction scheme where ethyl chloride is an intermediate product which is produced from the reaction of dichloroethane with hydrogen. The intermediate chlorine-containing product can be further hydrodechlorinated to ethane. Results obtained with the monometallic sample X0 (Fig. 11a) show that this mechanism can apply for palladium which mainly produces C_2H_6 and HCl as well as small amounts of CH_3–CH_2Cl at 200–300°C. The low selectivity in C_2H_4 at higher temperature is also in agreement with this scheme in which ethylene appears as a surface intermediate which is further hydrogenated to ethane. A high temperature may indeed provide sufficient energy for adsorbed C_2H_4 to return to the gas phase. As with the Rh/SiO_2 catalyst, the selectivity for C_2H_6 increases with increasing temperature from 200 to 250°C.

Campbell and Kemball (47) examined the catalytic hydrogenolysis of ethyl chloride over a palladium film between 100 and 200°C and found that Pd causes CH_3–CH_2Cl to decompose by the following reaction: CH_3–$CH_2Cl + H_2 \rightarrow C_2H_6 + HCl$. On nickel and iron films at higher temperatures (284 and 263°C, respectively), ethylene production by CH_3–$CH_2Cl \rightarrow C_2H_4 + HCl$ was additionally observed. Products detected with the X0 catalyst below 350°C are in agreement with the first reaction. The fact that, from 300 to 350°C, the decrease in ethyl chloride selectivity corresponds almost exactly to the increase in ethylene selectivity suggests that ethylene production over X0 may occur according to the second reaction.

The structure sensitivity of C–Cl hydrogenolysis has been pointed out by several authors (48–50) and could explain the catalytic results presented in Fig. 11. While a test with xerogel X100 showed that silver is completely inactive for the hydrodechlorination of 1,2-dichloroethane, the alloying of this metal with palladium, which has been reported to be the most active hydrodechlorination catalyst (51), leads to drastic changes in selectivity. The ensemble size concept (52–54) may explain the increasing and decreasing selectivities in C_2H_4 and C_2H_6, respectively, with increasing Ag content of the Pd–Ag alloy. As explained by Sinfelt (23), in the case of the hydrogenolysis of hydrocarbons over bimetallic catalysts, this selectivity effect may be explained by the hypothesis that the production of C_2H requires a surface site consisting of an array of adjacent active metal atoms which is larger than that required for C_2H_4 production. Diluting active Pd atoms in an alloy with increasing contents of inert Ag would then favor C_2H_4 rather than C_2H_6. However, explanations for the influence of silver on the selectivity of Pd–Ag alloys other than the one based on ensemble size can be advanced. The composition of mixed ensembles Pd–Ag could be the factor influencing the selectivity as explained by Ponec and Bond (55) or a bifunctional mechanism could be involved. Let us consider for example the following mechanism: Ag interacts with CH_2Cl–CH_2Cl and picks up chlorine atoms but does not hold the rest of the molecule ($\cdot CH_2$–$CH_2\cdot$) firmly enough and this fragment is released as ethylene; Ag alone is inactive because AgCl covers the surface and deactivates it; the AgCl surface cannot adsorb hydrogen but Pd can supply hydrogen atoms for its reduction into Ag; Pd splits the C–Cl bond too but Cl can be removed by hydrogen always coadsorbed with dichloroethane; ethylene can react with abundant H_{ads} up to ethane. It appears then that many mechanisms are possible and the catalytic data presented here do not allow one to discriminate between them. This point will be the subject of a further study.

Deactivation is observed with all catalysts but becomes slower when the Ag loading is increased and is scarcely distinguishable with sample X67. Poisoning during hydrodechlorination has been explained by the formation of a stable surface chloride (7, 48, 56), possibly with simultaneous coking (5). It has also been shown that the presence of Cl on Rh/SiO_2 decreases the hydrogenation activity of rhodium (5) which, in the case of palladium, may explain the increasing ethylene selectivity with time at the same temperature as observed with catalysts X33 and X50 (Figs. 11b and 11c).

CONCLUSIONS

The preparation method described in this study allows us to obtain low-density xerogel catalysts containing small Pd–Ag alloy particles which seem to be located inside microporous SiO_2 particles. At low contents of silver, the composition of the bimetallic particles is nearly the same as the overall composition and some pure silver particles are also observed. In xerogels richer in Ag, the percentage of this metal in the alloy particles is appreciably lower than the overall content. When dried under vacuum, xerogels exhibit pore volumes and pore size distributions similar to aerogels. The mechanism of gel formation seems to depend on the basicity of the solution, which probably strongly influences the structure of the silica network. The formation of the Pd–Ag alloy seems to occur by migration of silver through the pore structure and combination with palladium particles trapped inside silica particles. While hydrodechlorination of 1,2-dichloroethane over pure palladium mainly produces ethane, dilution of this active metal with silver leads to a strong increase in the ethylene selectivity.

In a future paper, the diffusion of reactants inside the porous structure of those bimetallic xerogels will be examined (sample X67, 1.5% Pd–3% Ag, will be chosen for its high ethylene selectivity). Textural analysis shows that the catalysts are composed of overlapping entities having various textures: silica particles are basic blocks which constitute aggregates, themselves constituents of catalyst pellets. In order to reach the active sites, reactants have to diffuse through a continuous distribution of macro- and mesopores and then through micropores inside silica particles. A comparison of diffusion coefficients and reaction rates will show that the xerogel catalysts prepared here exhibit remarkable mass transfer properties. A kinetic study of the hydrodechlorination of 1,2-dichloroethane over xerogel X67 will be the subject of further work, and the mechanism of the reaction will be examined.

ACKNOWLEDGMENTS

The authors warmly thank Mr. C. Lebrun, from the Solvay Company, for his invaluable help during the catalytic experiments, as well as Mr. R. Pirard and Professor A. Rulmont, from the University of Liège, for helpful discussions. B. Heinrichs is grateful to the Fonds pour la Formation à la Recherche dans l'Industrie et dans l'Agriculture, F.R.I.A., for financial support. The Ministère de la Région Wallonne—Direction générale des Technologies et de la Recherche, the Service de la Programmation de la Politique Scientifique, and the Fonds National de la Recherche Scientifique are also gratefully acknowledged for financial support.

REFERENCES

1. Ritter, E. R., Bozzelli, J. W., and Dean, A. M., *J. Phys. Chem.* **94**, 2493 (1990).
2. Kosusko, M., Mullins, M. E., Ramanathan, K., and Rogers, T. N., *Environ. Prog.* **7**, 136 (1988).
3. Tichenor, B. A., and Palazzolo, M. A., *Environ. Prog.* **6**, 172 (1987).
4. Kalnes, T. N., and James, R. B., *Environ. Prog.* **7**, 185 (1988).
5. Bozzelli, J. W., Chen, Y.-M., and Chuang, S. S. C., *Chem. Eng. Comm.* **115**, 1 (1992).
6. Fung, S. C., and Sinfelt, J. H., *J. Catal.* **103**, 220 (1987).
7. Anderson, J. R., and McConkey, B. H., *J. Catal.* **11**, 54 (1968).
8. Ito, L. N., Harley, A. D., Holbrook, M. T., Smith, D. D., Murchison, C. B., and Cisneros, M. D., International Patent Application WO 94/07827 (1994).
9. López, T., López-Gaona, A., and Gómez, R., *J. Non-Cryst. Solids* **110**, 170 (1989).
10. López, T., López-Gaona, A., and Gómez, R., *Langmuir* **6**, 1343 (1990).
11. López, T., Bosch, P., Asomoza, M., and Gómez, R., *J. Catal.* **133**, 247 (1992).
12. López, T., Gómez, R., Novaro, O., Ramírez-Solís, A., Sánchez-Mora, E., Castillo, S., Poulain, E., and Martínez-Magadán, J. M., *J. Catal.* **141**, 114 (1993).
13. López, T., Asomoza, M., Bosch, P., Garcia-Figueroa, E., and Gómez, R., *J. Catal.* **138**, 463 (1992).
14. López, T., Romero, A., and Gómez, R., *J. Non-Cryst. Solids* **127**, 105 (1991).
15. Breitscheidel, B., Zieder, J., and Schubert, U., *Chem. Mater.* **3**, 559 (1991).
16. Schubert, U., Breitscheidel, B., Buhler, H., Egger, C., and Urbaniak, W., *in* "Better Ceramics Through Chemistry V: Symp. Proc., San Francisco, April 27–May 1, 1992" (M. J. Hampden-Smith, W. G. Klemperer, and C. J. Brinker, Eds.), Materials Research Society Symposium Proceedings, Vol. 271, p. 621, Materials Research Society, Pittsburgh, 1992.
17. Schubert, U., *New J. Chem.* **18**, 1049 (1994).
18. Mörke, W., Lamber, R., Schubert, U., and Breitscheidel, B., *Chem. Mater.* **6**, 1659 (1994).
19. Kaiser, A., Görsmann, C., and Schubert, U., *J. Sol-Gel Sci. Technol.* **8**, 795 (1997).
20. Heinrichs, B., Pirard, J.-P., and Pirard, R., U.S. Patent 5,538,931 (1996).
21. Heinrichs, B., Noville, F., and Pirard, J.-P., *J. Catal.* **170**, 366 (1997).
22. Brinker, C. J., and Scherer, G. W., "Sol-Gel Science: The Physics and Chemistry of Sol-Gel Processing," Academic Press, San Diego, 1990.
23. Sinfelt, J. H., "Bimetallic Catalysts—Discoveries, Concepts, and Applications," Wiley, New York, 1983.
24. El Hamdaoui, A., Bergeret, G., Massardier, J., Primet, M., and Renouprez, A., *J. Catal.* **148**, 47 (1994).
25. Bouwman, R., Lippits, G. J. M., and Sachtler, W. M. H., *J. Catal.* **25**, 350 (1972).
26. Wood, B. J., and Wise, H., *Surf. Sci.* **52**, 151 (1975).
27. Kuijers, F. J., and Ponec, V., *J. Catal.* **60**, 100 (1979).
28. Allison, E. G., and Bond, G. C., *Catal. Rev.* **7**, 233 (1972).
29. Brunauer, S., Deming, L. S., Deming, W. S., and Teller, E., *J. Amer. Chem. Soc.* **62**, 1723 (1940).
30. Lecloux, A. J., *in* "Catalysis: Science and Technology" (J. R. Anderson and M. Boudart, Eds.), Vol. 2, p. 171, Springer, Berlin, 1981.
31. Rouquerol, J., Avnir, D., Fairbridge, C. W., Everett, D. H., Haynes, J. H., Pernicone, N., Ramsay, J. D. F., Sing, K. S. W., and Unger, K. K., *Pure Appl. Chem.* **66**, 1739 (1994).
32. Mikhail, R. S., Brunauer, S., and Bodor, E. E., *J. Colloid Interface Sci.* **26**, 45, 54 (1968).
33. Brunauer, S., *Chem. Eng. Progr. Symp. Ser. N°96* **65**, 1 (1969).
34. Broekhoff, J. C. P., and de Boer, J. H., *J. Catal.* **9**, 8 (1967).
35. Broekhoff, J. C. P., and de Boer, J. H., *J. Catal.* **9**, 15 (1967).
36. Broekhoff, J. C. P., and de Boer, J. H., *J. Catal.* **10**, 153 (1968).
37. Pirard, R., Blacher, S., Brouers, F., and Pirard, J.-P., *J. Mater. Res.* **10**, 2114 (1995).
38. Pirard, R., Heinrichs, B., and Pirard, J.-P., *in* "Characterisation of Porous Solids IV" (B. McEnaney, T. J. Mays, J. Rouquerol, F. Rodriguez-Reinoso, K. S. W. Sing, and K. K. Unger, Eds.), The Royal Society of Chemistry, London, in press.

39. Pirard, R., and Pirard, J.-P., *J. Non-Cryst. Solids* **212**, 262 (1997).
40. Pajonk, G. M., *Appl. Catal.* **72**, 217 (1991).
41. Yamane, M., *in* "Sol-Gel Technology for Thin Films, Fibers, Preforms, Electronics and Specialty Shapes" (L. C. Klein, Ed.), p. 200, Noyes Publications, Park Ridge, NJ, 1988.
42. Iler, R. K., "The Chemistry of Silica," Wiley, New York, 1979.
43. Coltrain, B. K., Melpolder, S. M., and Salva, J. M., *in* "Proceedings of the IVth International Conference on Ultrastructure Processing of Ceramics, Glasses, and Composites" (D. R. Uhlmann and D. R. Ulrich, Eds.), Wiley, New York, 1989.
44. Stevenson, S. A., Dumesic, J. A., Baker, R. T. K., and Ruckenstein, E., "Metal–Support Interactions in Catalysis, Sintering, and Redispersion," Van Nostrand–Reinhold, New York, 1987.
45. Ruckenstein, E., and Pulvermacher, B., *J. Catal.* **37**, 416 (1975).
46. Zou, W., and Gonzalez, R. D., *Appl. Catal. A* **126**, 351 (1995).
47. Campbell, H. S., and Kemball, C., *Trans. Faraday Soc.* **57**, 809 (1961).
48. Coq, B., Ferrat, G., and Figueras, F., *J. Catal.* **101**, 434 (1986).
49. Coq, B., Ferrat, G., and Figueras, F., *React. Kinet. Catal. Lett.* **27**, 157 (1985).
50. Fouilloux, P., Cordier, G., and Colleuille, Y., *Stud. Surf. Sci. Catal.* **11**, 369 (1982).
51. Rylander, P. N., "Catalytic Hydrogenation over Platinum Metals," Academic Press, New York, 1967.
52. Thomas, J. M., and Thomas, W. J., "Principles and Practice of Heterogeneous Catalysis," VCH, Weinheim, 1997.
53. Soma-Noto, Y., and Sachtler, W. M. H., *J. Catal.* **32**, 315 (1974).
54. Dowden, D. A., *in* "Proceedings of the 5th International Congress on Catalysis" (J. W. Hightower, Ed.), 1973.
55. Ponec, V., and Bond, G. C., "Catalysis by Metals and Alloys," Elsevier, Amsterdam, 1995.
56. Kovenklioglu, S., Cao, Z., Shah, D., Farrauto, R. J., and Balko, E. N., *AIChE J.* **38**, 1003 (1992).